Microbiological Research 292 (2025) 128043

Contents lists available at ScienceDirect

Microbiological Research

journal homepage: www.elsevier.com/locate/micres

The *Actinobacillus pleuropneumoniae apxIV* operon encodes an antibacterial toxin-immunity pair

Eva Slivenecka, David Jurnecka, Jana Holubova, Ondrej Stanek, Ludmila Brazdilova, Monika Cizkova, Ladislav Bumba *

Institute of Microbiology of the Czech Academy of Sciences, Videnska 1083, Prague 142 00, Czech Republic

ARTICLE INFO

Keywords:
RTX proteins
Actinobacillus pleuropneumoniae
Toxin-antitoxin system
Bacterial
Pathogenesis
Infectious Diseases
Structural biology

ABSTRACT

The ApxIVA protein belongs to a distinct class of a "clip and link" activity of Repeat-in-ToXin (RTX) exoproteins. Along with the three other pore-forming RTX toxins (ApxI, ApxII and ApxIII), ApxIVA serves as a major virulence factor of *Actinobacillus pleuropneumoniae*, the causative agent of porcine pneumonia. The gene encoding ApxIVA is located on a bicistronic operon downstream of the *orf1* gene and is expressed exclusively under *in vivo* conditions. Both ApxIVA and ORF1 are essential for full virulence of *A. pleuropneumoniae*, but the molecular mechanisms by which they contribute to the pathogenicity are not yet understood. Here, we provide a comprehensive structural and functional analysis of ApxIVA and ORF1 proteins. Our findings reveal that the N-terminal segment of ApxIVA shares structural similarity with colicin M (ColM)-like bacteriocins and exhibits an antimicrobial activity. The ORF1 protein resembles the colicin M immunity protein (Cmi) and, like Cmi, is exported to the periplasm through its N-terminal signal peptide. Additionally, ORF1 can protect bacterial cells from the antimicrobial activity of ApxIVA, suggesting that ORF1 and ApxIVA function as an antibacterial toxin-immunity pair. Moreover, we demonstrate that fetal bovine serum could elicit ApxIVA and ORF1 production under *in vitro* conditions. These findings highlight the coordinated action of various RTX determinants, where the fine-tuned spatiotemporal production of ApxIVA may enhance the fitness of *A. pleuropneumoniae,* facilitating its invasion to a resident microbial community on the surface of airway mucosa.

1. Introduction

The Repeats in ToXin (RTX) family constitutes a distinct class of bacterial proteins that are secreted into the extracellular medium by a type I secretion system (T1SS). The RTX substrates feature non-cleavable C-terminal secretion signal, which is preceded by a variable number of glycine- and aspartate-rich nonapeptide tandem repeats with the consensus sequence motif GGxGxDxxx (Linhartova et al., 2010). At low concentrations of calcium ions in the bacterial cytosol (<100 nM), the RTX repeats remain intrinsically unstructured and only fold outside of the bacterial cell upon exposure to (sub)millimolar concentrations of Ca^{2+} ions into a functional Ca^{2+}-loaded structure known as a parallel β-roll (Baumann, 2019; Domínguez et al., 2015; Motlova et al., 2020). The process of folding progresses successively from the carboxy toward amino terminus of the RTX repeats and plays a crucial role in the secretion of very large RTX polypeptides (Bumba et al., 2016). The RTX proteins display a diverse range of biological activities, spanning from the historically first characterized pore-forming RTX toxins (Benz, 2016; Frey, 2019; Ristow and Welch, 2019), through the large multifunctional-autoprocessing RTX toxins (MARTX) (Gavin and Satchell, 2015; Woida and Satchell, 2018), adhesins (Guo et al., 2019; Smith et al., 2018), surface layer proteins (Sleytr et al., 2014), bacteriocins (Venter et al., 2001), nodulation proteins (Yasuta et al., 2001), secreted hydrolytic enzymes exhibiting metalloprotease or lipase activities (Baumann et al., 1993; Meier et al., 2007), up to RTX proteins of unknown biological function (Linhartova et al., 2010).

Actinobacillus pleuropneumoniae, the predominant Gram-negative pathogen implicated in porcine respiratory infections, produces four closely related Apx exoproteins classified within the RTX protein family (Bosse et al., 2002; Chiers et al., 2010; Sassu et al., 2018; Soto Perezchica et al., 2023; Stringer et al., 2022). ApxI, ApxII and ApxIII are prototypical pore-forming RTX toxins, exhibiting strong hemolytic and cytotoxic activities, and serve as key virulence factors of *A. pleuropneumoniae* (Benz, 2016; Frey and Kuhnert, 2002; Maier et al.,

* Corresponding author.
E-mail address: bumba@biomed.cas.cz (L. Bumba).

https://doi.org/10.1016/j.micres.2024.128043
Received 1 September 2024; Received in revised form 20 December 2024; Accepted 24 December 2024
Available online 26 December 2024

1996; Ristow and Welch, 2019). These toxins are initially synthesized as inactive protoxins that undergo post-translational activation before being exported from the bacterial cell (Stanley et al., 1998). This activation involves a post-translational modification of ε-amino groups of internal lysine residues within conserved acylation sites through covalent attachment of amide-linked fatty acyl residues. This reaction is catalyzed by an acyltransferase encoded by the *C* gene, which is co-expressed with the protoxin structural gene (*A*) and the secretion apparatus-encoding genes (*B* and *D)* within a prototypical *apxCABD* operon (Fig. 1). The acyltransferase enzyme selects an acyl chain of a specific length (Osickova et al., 2020), and the acylation of at least one out of two lysine residues of the protoxin is essential for its biological activity (Ludwig et al., 1996; Stanley et al., 1994).

The fourth RTX species, ApxIVA, distinguishes itself from other Apx toxins through several unique features: 1) it is highly specific to *A. pleuropneumoniae*; 2) it is produced by all *A. pleuropneumoniae* strains (currently 18 serotypes); and 3) it is exclusively expressed under *in vivo* conditions (Liu et al., 2009; Nahar et al., 2021; Schaller et al., 1999). Consequently, these characteristics have positioned ApxIVA as a valuable tool for serodiagnosis of infections and surveillance of *A. pleuropneumoniae* within pig herds (Dreyfus et al., 2004; Gottschalk, 2015; Stringer et al., 2022). ApxIVA is an RTX protein of variable length (1805 residues in the strain 4074, serovar 1) encoded in a bicistronic operon downstream of the *orf1* gene (Schaller et al., 1999). The *orf1* gene product (ORF1) was proposed to play a role in the weak hemolytic activity of ApxIVA (Schaller et al., 1999) and in maintaining of full virulence of *A. pleuropneumoniae* (Yuan et al., 2011). However, the specific biological role of ORF1 remains unclear. ApxIVA exhibits an autocatalytic "clip and link" activity that involves Ca^{2+}-dependent processing of the Asp_{638}-Pro_{639} peptide bond and covalent linkage of the released carboxyl group of Asp_{638} to an adjacent ε-amino group of another lysine residue through an Asp-Lys isopeptide bond (Kuban et al., 2020; Osicka et al., 2004). This process is orchestrated by the Ca^{2+}-induced conformational rearrangement of a self-processing module (SPM), which encompasses a highly homologous region adjacent to the cleavage site (residues 639–816), and thereby defines a specific subset of the self-processed RTX proteins (Matyska Liskova et al., 2016). Deletion of the SPM from the ApxIVA polypeptide decreases the virulence of *A. pleuropneumoniae* in the pig infection model (Kuban et al., 2020). However, the molecular mechanisms underlying the ApxIVA-mediated virulence remain to be fully elucidated.

Here, we present a comprehensive structural and functional analysis of the ApxIVA and ORF1 proteins. Our findings demonstrate that the N-terminal domain of ApxIVA exhibits antimicrobial activity and, together with ORF1, which is exported to the periplasm, likely constitutes an antibacterial toxin-immunity pair. Additionally, we describe straightforward and reproducible cultivation conditions that enable the production of ApxIVA and ORF1 in *A. pleuropneumoniae* under *in vitro* conditions.

2. Results

2.1. ApxIVA is free of fatty acid acylation on internal lysine residues

Primary amino acid sequence of the ApxIVA protein contains three GK dipeptides that could potentially be targets for acylation; the first (K_{790}) located within the C-terminal of SPM, the second (K_{1000}) in the central domain, and the third (K_{1247}) situated in the N-terminal part of the RTX domain (Fig. 2A). To analyze the acylation status of ApxIVA, the His-tagged ApxIVA protein was expressed in *E. coli* cells alone or co-expressed in the presence of the ORF1 protein and the *A. pleuropneumoniae* ApxIC, ApxIIC and ApxIIIC acyltransferases (Fig. 2B). Mass spectrometry analysis of tryptic digests of the purified proteins revealed that all five distinct ApxIVA preparations generated the $_{776}$NDFLAGNNILAQLG**K**$_{790}$ and $_{1235}$DHADWDSILEGG**K**$_{1247}$ peptides, indicating that neither K_{790} nor K_{1247} harbored any post-translational modification (Fig. 2C). For the K_{1000} residue, no mass corresponding to the anticipated $_{996}$QFEGK$_{1000}$ peptide was recovered in our analyses. However, the consecutive peptide $_{1001}$WVTDYSR$_{1007}$ was unambiguously identified in the tryptic digests of all five ApxIVA preparations. Given that the $_{1001}$WVTDYSR$_{1007}$ complies well with trypsin cleavage rules (Arg/Lys-↓-X), we can conclude that the K_{1000}

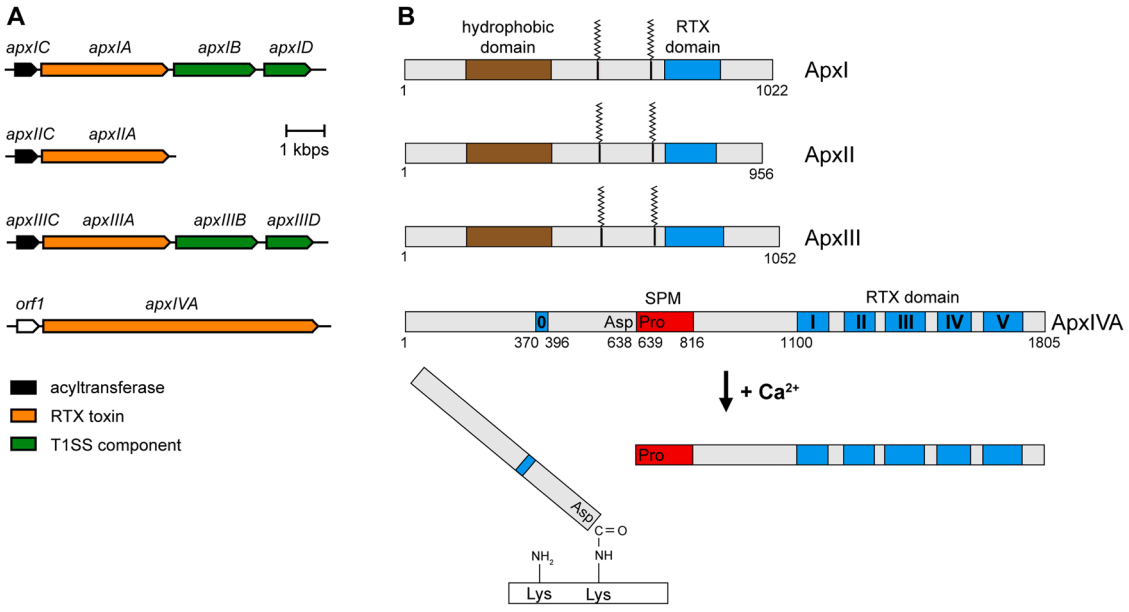

Fig. 1. (A) The schematic representation of the *apx* gene clusters of *Actinobacillus pleuropneumoniae*. The arrows represent coding regions and transcriptional directions of the genes deposited under the GenBank accession number (CP029003.1). (B) Domain structures of the *A. pleuropneumoniae* Apx proteins. Sites of post-translational modification of internal lysines of the ApxI, ApxII, ApxIII toxins by covalent attachment of fatty acyl chains are indicated. The ApxIVA protein undergoes Ca^{2+}-induced autocatalytic processing mediated by a self-processing module (SPM, in red) located downstream of the cleavage site (residues 639–816). This involves the processing of the D_{638}-P_{639} peptide bond and covalent linkage of the released D_{638} residue to an ε-amino group of a neighboring lysine residue through an Asp-Lys isopeptide bond. Individual blocks of RTX repeats are colored in blue and numbered.

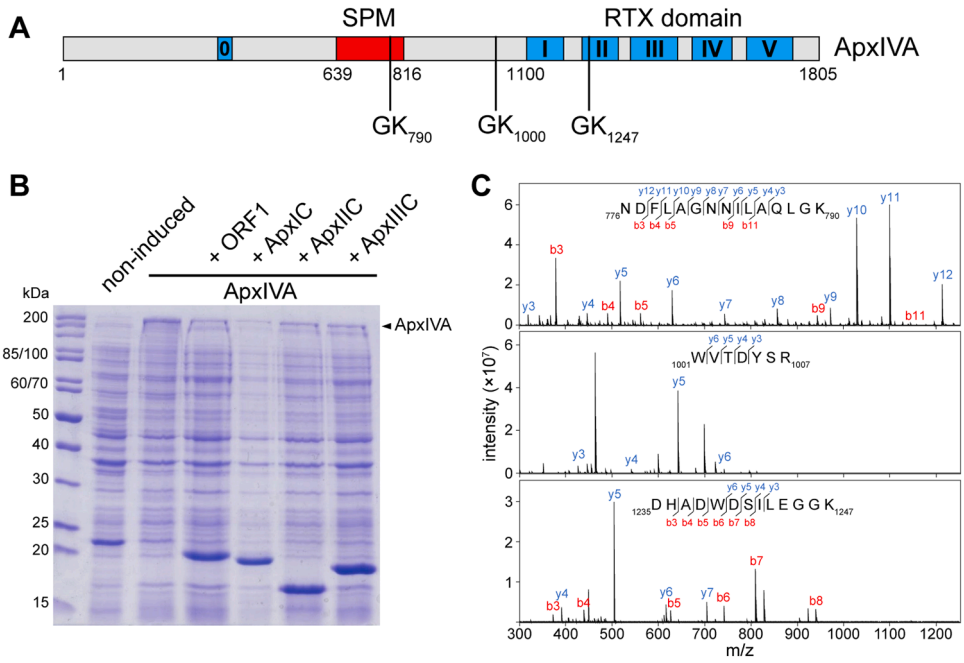

Fig. 2. ApxIVA is not acylated on internal lysine residues. (A) The schematic representation of the ApxIVA protein. The location of putative acylation sites (GK dipeptide) is indicated. (B) SDS-PAGE analysis of cell lyzates of the IPTG-induced *E. coli* BL21 λDE3 cells producing ApxIVA alone, or ApxIVA co-expressed in the presence of ORF1 or the ApxIC, ApxIIC or ApxIIIC acyltransferases. The protein samples were separated on 12 % gels and stained with a Coomassie Blue. (C) MS/MS spectrum of the tryptic peptides [776–790], [1001–1007] and [1235–1247] of the recombinant ApxIVA protein co-expressed in *E. coli* BL21 λDE3 in the presence of the ORF1 protein. The peptide sequence is shown on the top with the collision-induced fragmentation pattern. The b and y ions are shown in red and blue, respectively. The data are representative of two independent experiments.

residue does not possess any posttranslational modification. Additionally, none of the peptides recovered from all ApxIVA preparations showed evidence of acylation. Since the recombinant ApxIVA protein lacks fatty acid acylation on its internal lysine residues, it is likely that the native ApxIVA secreted by *A. pleuropneumoniae* is also not acylated.

2.2. Structural characterization of the N-terminal domain of ApxIVA

Analysis of the primary amino acid sequence of $ApxIVA_{1–638}$ revealed no significant similarity to any known protein sequences, except for the presence of two consecutive nonapeptide RTX motifs located between residues 370–378 and 388–396 (designated as RTX block 0, see Fig. 1B). A *de novo* protein structure prediction using AlphaFold (Abramson et al., 2024) demonstrated that these RTX motifs form a characteristic right-handed helix of parallel β-strands, also known as a β-roll; a structural hallmark of RTX repeats (Fig. 3A). This β-roll structure interconnects an α-helical N-terminal domain (residues 1–365) with an antiparallel β-sheet structure (residues 420–550) and a long unstructured region (residues 551–638) at the C-terminus of the polypeptide. Structural similarity search using DALI (Holm et al., 2023) revealed that the predicted $ApxIVA_{1–638}$ structure does not resemble any structures deposited in the Protein Data Bank (PDB; www.rcsb.org). The closest structural matches to $ApxIVA_{1–638}$ were identified to be an alkaline protease of *Pseudomonas aeruginosa* (Ravaud et al., 2003) and colicin-like bacteriocins, such as pectocin M2 (Grinter et al., 2014) or colicin M (Zeth et al., 2008). However, the overall structural similarity was very low, with DALI Z-scores below 7.1 and more than 3.4 Å displacements of main chain atoms in aligned secondary structures (Supplementary Fig. S1).

To investigate the structural and functional characteristics of $ApxIVA_{1–638}$ in more detail, we prepared a recombinant truncated protein, $ApxIVA_{1–570}$, which lacks the unstructured C-terminal segment. The $ApxIVA_{1–570}$ protein was recovered from inclusion bodies after solubilization with 8 M urea and refolded into a native state by rapid dilution. This process yielded a monomeric form of $ApxIVA_{1–570}$, as evidenced by a single peak on size exclusion chromatography with retention time corresponding to a globular protein of ~60 kDa (Fig. 3B). The far-UV circular dichroism (CD) spectrum of the refolded $ApxIVA_{1–570}$ protein exhibited a negative band at 208 nm with a shoulder at 222 nm, indicating the presence of α-helices and β-sheets in the protein structure (Fig. 3C). Titration of $ApxIVA_{1–570}$ with calcium ions did not induce significant changes in the CD spectra, suggesting that Ca^{2+} ions are dispensable for folding of the $ApxIVA_{1–570}$ protein (Fig. 3C).

2.3. Structural characterization of the ORF1

Inspection of the 157-residue long sequence of ORF1 using Phobius (Käll et al., 2004) indicated the presence of a putative N-terminal secretory signal peptide, promoting ORF1 export to the periplasm. Moreover, the signal peptide of ORF1 was predicted to harbor two processing sites recognized by type I general signal peptidase: the major one between Tyr_{19} and Ala_{20} and the minor one between residues Trp_{21} and Tyr_{22}. To determine whether the putative ORF1 signal peptide facilitates protein export into the periplasm, we constructed a series of plasmids containing genetic fusion with the signal-less enzymatic domain of the *E. coli* alkaline phosphatase ($PhoA_{23–471}$). The PhoA activity, which occurs exclusively in the oxidative environment of the periplasm and not in the reducing cytoplasm of bacteria, was assessed by monitoring the conversion of the chromogenic substrate 5-bromo-4-chloro-3-indolyl phosphate (BCIP) to a blue product (Hoffman and Wright, 1985). As shown in Fig. 4A, bacteria expressing the $ORF1_{1–25}$-$PhoA_{23–471}$ fusion construct produced dark-blue colonies, comparable to those formed by bacteria expressing the full-length PhoA enzyme ($PhoA_{1–471}$). In contrast, bacteria expressing either PhoA-free ORF1 ($ORF1_{1–157}$) or $PhoA_{23–471}$ alone produced colorless colonies on BCIP plates. These results indicated that the first 25 residues of ORF1 function as an N-terminal signal peptide, facilitating the protein export into the bacterial periplasm.

To further characterize the ORF1, we first sought to purify ORF1 as a

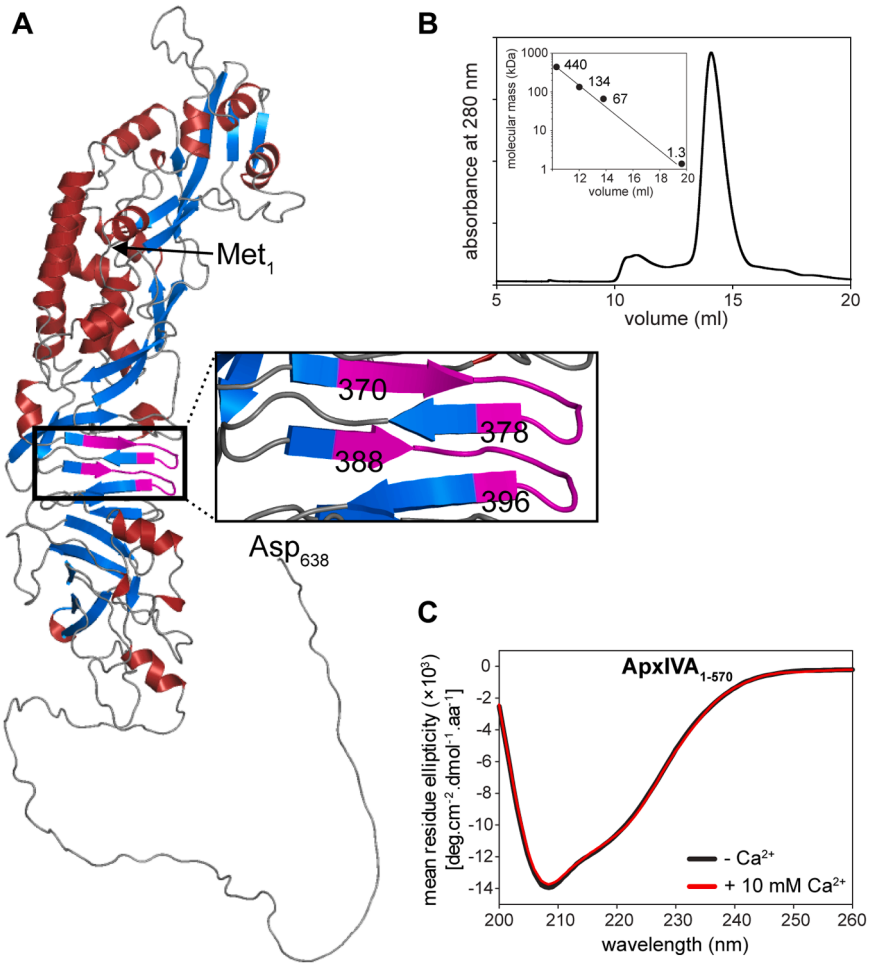

Fig. 3. Structural and functional characterization of the ApxIVA$_{1–570}$ protein. (A) AlphaFold prediction of the ApxIVA$_{1–638}$ structure. The α-helices and β-sheets are colored in red and blue, respectively. The inset represents a close-up view of two consecutive nonapeptide RTX motifs (residues 370–378 and 388–396) arranged in parallel β-roll structure. The side chains of aspartate residues within the conserved GGxGxDxxx motif are indicated. The carbon and oxygen atoms are colored in gray and red, respectively. (B) Size exclusion chromatography of ApxIVA$_{1–570}$. The purified protein (1 mg in 500 μl) was injected onto a Superdex 200 Increase column and the chromatogram was recorded at 280 nm. Inset, the calibration curve of protein standards: apoferritin (443 kDa), bovine serum albumin (134 and 67 kDa), and vitamin B12 (1.3 kDa). (C) Far-UV CD spectra of ApxIVA$_{1–570}$ in the absence (-Ca^{2+}) and in the presence of 10 mM $CaCl_2$.

soluble recombinant protein. Initial attempts to prepare a signal-less ORF1 protein (ORF1$_{23–157}$) were hindered by the insolubility of the expressed protein and its inability to refold as a native protein. This issue was likely attributed to protein misfolding caused by aberrant disulfide pairing of four cysteine residues occurring in the ORF1 sequence. To address the problem of improper disulfide bond formation upon refolding *in vitro*, we expressed ORF1$_{23–157}$ as a fusion protein with an N-terminal pelB signal peptide (guiding protein export to the periplasm) and purified the signal-less ORF1$_{23–157}$ protein from the periplasm of *E. coli* cells. Size exclusion chromatography revealed that the purified ORF1$_{23–157}$ elutes as a monomeric protein with a molecular weight of about 16 kDa (Fig. 4B). The far-UV CD spectrum of ORF1$_{23–157}$ displayed two negative bands at 208 nm and 218 nm, indicating a mixture of α-helical and β-sheets structures (Fig. 4C). Despite numerous attempts, the atomic structure of ORF1$_{23–157}$ was not determined due to failure to obtain diffracting crystals or well-resolved NMR spectra.

The structure prediction by AlphaFold revealed that ORF1$_{23–157}$ likely comprises a four-stranded antiparallel β-sheet diagonally crossed by a five-turn α-helix (Fig. 4D). The structural model includes a disulfide bond between the Cys_{36} and Cys_{147} residues, linking the N- and C-terminal portions of the protein. Indeed, the presence of a Cys_{36}-Cys_{147} disulfide bond in ORF1$_{23–157}$ was demonstrated by differential MALDI-TOF peptide mass fingerprinting using reduced and non-reduced conditions combined with subsequent digestion with trypsin (Fig. 4E). Furthermore, the N-terminal truncation of ORF1$_{23–157}$ (ORF1$_{38–157}$) resulted in the formation of protein aggregates, indicating that the Cys_{36}-Cys_{147} disulfide bond is critical for the stability of ORF1$_{23–157}$ (Fig. 4B). Structural similarity search using DALI (Holm et al., 2023) revealed that the predicted ORF1$_{23–157}$ structure shares the highest structural similarity with the periplasmic domain of the DotI component of the *Legionella pneumophila* Dot/Icm type IV secretion system (Kuroda et al., 2015), cystatin C, a cysteine protease inhibitor (Bode et al., 1988), and the colicin M immunity protein (Gérard et al., 2011). However, the overall structural similarity was relatively low, with DALI Z-scores below 4.9 and more than 2.9 Å displacements of main chain atoms in aligned secondary structures (Supplementary Fig. S2).

2.4. Fetal bovine serum (FBS), but not serum albumin, elicits production of ApxIVA and ORF1 in vitro

To examine the expression of ApxIVA and ORF1 proteins in *A. pleuropneumoniae* cells, we generated polyclonal antibodies by immunizing mice with recombinant full-length ApxIVA and ORF1$_{23–157}$ proteins, respectively. The expression of ApxIVA is generally considered to be attenuated under *in vitro* conditions until *A. pleuropneumoniae* encounters bronchoalveolar fluid or porcine lung tissue (Baltes and Gerlach, 2004; Lone et al., 2009). Initial attempts to induce the ApxIVA expression *in vitro* by supplementing the growth medium with

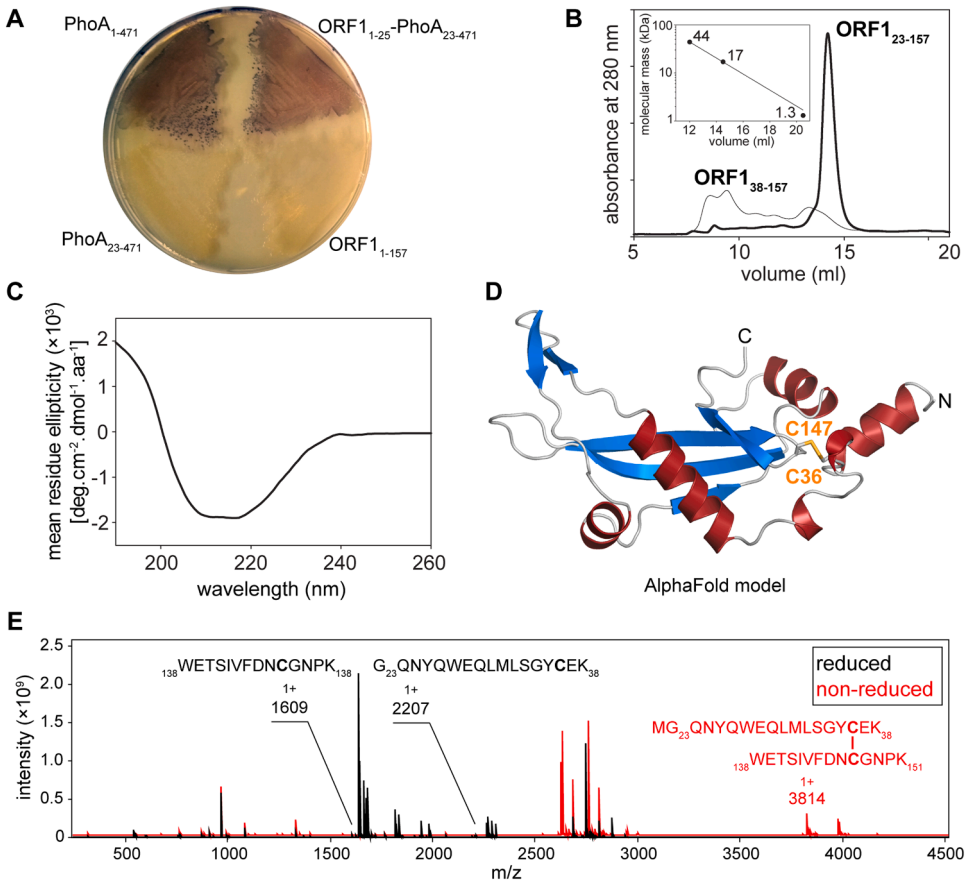

Fig. 4. Structural and functional characterization of the ORF1$_{23–157}$ protein. (A) Detection of alkaline phosphatase (PhoA) activity in the periplasm of *E. coli* XL1-Blue cells. The bacteria were transformed with indicated *phoA* fusions and grown on LB agar plates supplemented with a chromogenic PhoA substrate. The phosphatase activity was detected as a dark phenotype of colonies. (B) Size exclusion chromatography of ORF1$_{23–157}$ and ORF1$_{38–157}$. The purified proteins (~2 mg in 500 µl) were injected onto a Superdex 75 Increase column and the chromatogram was recorded at 280 nm. Inset, the calibration curve of protein standards: chicken ovalbumin (44 kDa), horse myoglobin (17 kDa), and vitamin B12 (1.3 kDa). (C) Far-UV CD spectrum of ORF1$_{23–157}$. (D) AlphaFold prediction of the ORF1$_{23–157}$ structure. The α-helices and β-sheets are colored in red and blue, respectively. Cysteine residues forming disulfide bridges are highlighted in orange. (E) MALDI-TOF spectra of ORF1$_{23–157}$ digested by trypsin under reducing (black) and non-reducing (red) conditions. The mass and sequence of the peptides containing cysteine residues are indicated.

sterile-filtered bronchoalveolar fluid or porcine lung cell extracts yielded inconsistent and non-reproducible results. To address this issue and replace porcine-derived components in the medium, we tested various laboratory-available alternatives. Among these, fetal bovine serum (FBS) proved fully effective in promoting the *in vitro* production of both ApxIVA and ORF1. As shown in Fig. 5, immunoblot analyses demonstrated that ApxIVA is released into the culture supernatant of *A. pleuropneumoniae* cells grown exclusively in TSB medium supplemented with 10 % FBS (TSB-FBS). The signal was specific, as no protein bands were detected in bacterium-free TSB-FBS. ApxIVA predominantly appeared in its processed form, with a prominent protein band at ~140 kDa corresponding to the carboxy-terminal fragment after its autocatalytic cleavage (Osicka et al., 2004). The full-length ApxIVA was also detected as ~205 kDa protein band but only in very low amounts (Fig. 5). Notably, supplementation of TSB-FBS with 2 mM Ca^{2+} ions resulted in the disappearance of the ~205 kDa protein band, indicating the calcium-dependent autocatalytic cleavage of the full-length ApxIVA. Furthermore, the addition of 2 mM Ca^{2+} ions in TSB-FBS significantly increased the amount of secreted ApxIVA in the culture supernatant, corroborating the previous report that calcium ions enhance the secretion efficiency of large RTX substrates (Bumba et al., 2016).

In parallel, the production of ORF1 was assessed in whole-cell extracts using immunoblots probed with polyclonal mouse serum raised against the recombinant ORF1$_{23–157}$ protein. As further shown in Fig. 5, ORF1 was detected in *A. pleuropneumoniae* cells grown in the presence of FBS. Unlike ApxIVA, the overall amount of ORF1 protein in cell lysates remained constant, irrespective of the Ca^{2+} levels in the growth medium. The anti-ORF1$_{23–157}$ serum recognized two distinct bands with molecular masses of approximately 15 and 17 kDa. Fractionation of the cells revealed that the 15-kDa band was exclusively localized to the periplasmic fraction, while the 17-kDa band was found in the bacterial cytosol (Fig. 5). These findings suggested that ORF1 is synthesized as a 17-kDa precursor polypeptide, which undergoes signal peptide processing to yield a mature 15-kDa protein upon export to the periplasm.

To identify the component(s) in FBS responsible for inducing the production of ApxIVA and ORF1 proteins, FBS was fractionated into low (<3 kDa) and high (>3 kDa) molecular weight fractions using a 3 kDa cut-off membrane. As shown in Fig. 5, neither ORF1 nor ApxIVA was detected in cells grown with the low molecular weight fraction (<3 kDa). In contrast, cells grown in TSB supplemented with the high molecular weight fraction (>3 kDa) exhibited ORF1 and ApxIVA levels comparable to those observed in TSB-FBS. These results suggest that the higher molecular weight (proteinaceous) components of FBS, rather than the low molecular weight constituents, are responsible for inducing the production of ORF1 and ApxIVA in *A. pleuropneumoniae* cells. To investigate whether serum albumin has a potency to elicit the production of ORF1 and ApxIVA, *A. pleuropneumoniae* was cultured in the presence of bovine serum albumin (BSA) and analyzed as described above. As demonstrated in Fig. 5, neither ORF1 nor ApxIVA was detected in cells grown in the presence of different concentrations of

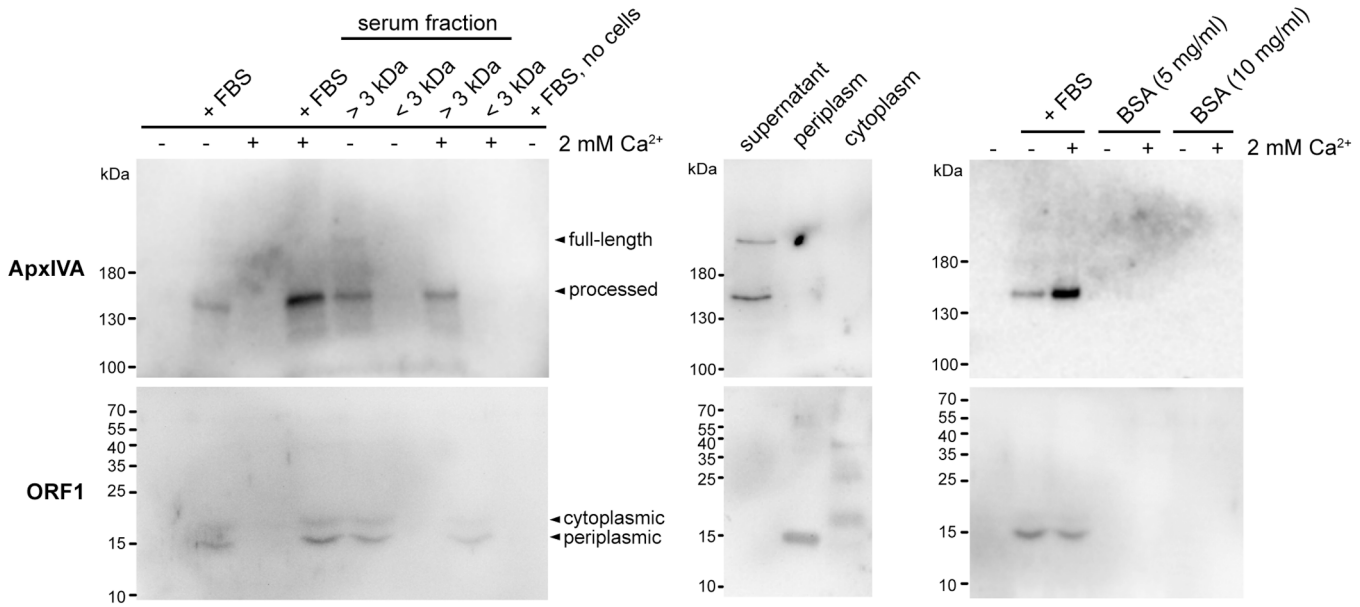

Fig. 5. Fetal bovine serum (FBS) elicits production of ApxIVA and ORF1 in *A. pleuropneumoniae* under *in vitro* conditions. Western blot analysis of ApxIVA (upper panels) and ORF1 (lower panels) production in *A. pleuropneumoniae*. The cells were cultivated at 37 °C in TSB medium alone or in TSB supplemented with the indicated compound(s) until an $OD_{600\ nm}$ of ~1.0 was reached. The cultures were then centrifuged at 20,000 g for 5 min to separate the culture supernatants and pelleted cells. The protein samples from the culture supernatants and pelleted cells were separated on 5 % (for ApxIVA detection) and 15 % (for ORF1 detection) SDS-polyacrylamide gels, respectively. The separated proteins were transferred to a nitrocellulose membrane and probed with mouse polyclonal sera raised against the recombinant ApxIVA and $ORF1_{23–157}$ proteins. The data are representative of at least three independent experiments.

BSA (up to 10 mg/ml), suggesting that serum albumin alone does not promote the production of ORF1 and ApxIVA in *A. pleuropneumoniae* cells.

2.5. *$ApxIVA_{1–570}$ exhibits an antimicrobial activity*

To elucidate the biological function of the N-terminal segment of ApxIVA, the enzymatic and cytotoxic activities of the recombinant $ApxIVA_{1–570}$ protein were evaluated. Functional *in vitro* enzymatic assays, using a Pierce Colorimetric Protease and EnzChek Phosphatase assay kits, revealed that $ApxIVA_{1–570}$ lacks both protease and phosphatase activities. Despite testing various experimental conditions (e.g., pH, temperature, metal ions) and $ApxIVA_{1–570}$ concentrations (up to 100 μg/μl), no enzymatic activity was detected (data not shown). Next, a potential pore-forming activity of $ApxIVA_{1–570}$ was assessed by examining its ability to puncture the cell membrane of sheep erythrocytes and release hemoglobin into the medium. Unlike ApxIA, which exhibits strong hemolytic activity, neither $ApxIVA_{1–570}$ nor full-length ApxIVA was capable of inducing hemolysis in erythrocytes (Fig. S3B). Additionally, a potential cytotoxicity of $ApxIVA_{1–570}$ against selected host cell types was evaluated using primary porcine alveolar macrophages (PPAMs) and newborn pig trachea (NPTr) cells. Here, cell viability was monitored in real-time using a CellTox Green uptake assay. In contrast to ApxIA, which also induces cytotoxicity in porcine macrophages, exposure to $ApxIVA_{1–570}$ or ApxIVA did not affect the viability of PPAMs (Fig. S3C, left panel). Similarly, the viability of NPTr cells remained unaffected following incubation with either $ApxIVA_{1–570}$ or ApxIVA, indicating that these proteins do not exhibit cytotoxic effect on host cells (Fig. S3C, right panel).

To explore a potential antimicrobial property of $ApxIVA_{1–570}$, its activity against a panel of Gram-negative (*Escherichia coli, Neisseria meningitidis, Bordetella pertussis*) and Gram-positive (*Bacillus subtilis, Streptococcus pneumoniae, Staphylococcus aureus*) bacteria was evaluated using a spot-on-lawn method. Among the tested strains, only the XL-1 Blue strain of *E. coli* exhibited sensitivity to $ApxIVA_{1–570}$, as indicated by zones of growth inhibition on top agar bacterial overlay (Fig. 6). The

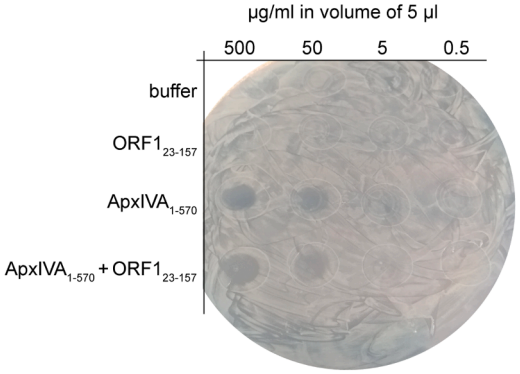

Fig. 6. $ApxIVA_{1–570}$ exhibits an antimicrobial activity. Spot-on-lawn assay of $ApxIVA_{1–570}$ and $ORF1_{23–157}$ against *E. coli* XL-1 Blue. LB agar plates freshly seeded with *E. coli* XL-1 Blue were spotted by tenfold serial dilutions of purified proteins and incubated overnight at 30 °C. The data are representative of the three independent experiments.

growth inhibition was concentration-dependent, with a minimal inhibitory concentration of approximately 50 μg/ml. These findings demonstrate that $ApxIVA_{1–570}$ possesses an antimicrobial activity.

2.6. *ORF1 enhances the fitness of A. pleuropneumoniae*

To assess the biological relevance of ORF1, the cytotoxic, protease-inhibitory, and antimicrobial-modulating activities of the recombinant $ORF1_{23–157}$ protein were tested. As shown in Supplementary Fig. 3, $ORF1_{23–157}$ neither caused hemolysis of erythrocytes nor affected the viability of PPAMs or NPTr cells, indicating that it does not exhibit cytotoxic activity towards host cells. Additionally, no inhibition of proteolytic activity was observed for selected cysteine proteases (papain, cathepsin B, or tobacco-etch virus protease) in the presence of $ORF1_{23–157}$, even at concentrations up to 100 μg/ml, suggesting that $ORF1_{23–157}$ does not appear to be a cysteine protease inhibitor (data not

shown). Next, a potential protective effect of $ORF1_{23–157}$ against the antimicrobial activity of $ApxIVA_{1–570}$ was tested using the spot-on-lawn method. As shown in Fig. 6, an equimolar mixture of $ORF1_{23–157}$ and $ApxIVA_{1–570}$ did not mitigate the growth inhibition of *E. coli* XL-1 Blue caused by $ApxIVA_{1–570}$. The lack of a protective effect is likely due to the inability of the recombinant $ORF1_{23–157}$ and $ApxIVA_{1–570}$ proteins to form a stable complex, as indicated by size exclusion chromatography (Supplementary Fig. S4A). On the other hand, structural modeling using MultiFold (McGuffin et al., 2023) predicted several potential interaction modes between $ApxIVA_{1–570}$ and $ORF1_{23–157}$. However, both global and local model quality estimates were low, suggesting uncertainty in the predicted interactions (Supplementary Fig. S4B).

To investigate the role of ORF1 *in vivo*, we prepared an in-frame deletion the *orf1* gene in the *A. pleuropneumoniae* chromosome. As expected, deletion of the *orf1* gene led to the loss of the ORF1 protein in the cell lysate of the Δ*orf1* mutant (Fig. 7A). On the other hand, comparable levels of secreted ApxIVA were detected in the culture supernatants of the Δ*orf1* mutant and parental strain, indicating that the lack of the *orf1* gene does not affect the capacity of the Δ*orf1* mutant to produce and secrete ApxIVA. To assess a potential protective effect of ORF1 against the killing activity of $ApxIVA_{1–570}$, sensitivity of the Δ*orf1* mutant against the parental strain was examined by a cross-streak assay. As shown in Fig. 7B, the Δ*orf1* mutant exhibited increased sensitivity to the parental strain than the parental strain to itself. This was evidenced by a pronounced zone of growth inhibition of the Δ*orf1* mutant in the proximity of the central streak formed by the parental strain. Additionally, the production of ApxIVA in the absence of ORF1 made the Δ*orf1* mutant more susceptible to growth inhibition compared to the parental strain, as demonstrated by a significant reduction in its growth rate of the Δ*orf1* mutant in TSB-FBS medium (Fig. 7C, right panel). In contrast, the growth rates of the Δ*orf1* mutant and the parental strains were comparable when cultured in TSB medium (Fig. 7C, left panel), indicating that the observed growth differences in TSB-FBS medium are due to ApxIVA activity rather than the mutation itself. These findings suggested that ORF1 enhances the fitness of *A. pleuropneumoniae* and likely contributes to resistance of bacterial cells against the antimicrobial activity of $ApxIVA_{1–570}$.

3. Discussion

ApxIVA represents one of the members of a 'clip-and-link' activity of RTX proteins that are characterized by the highly specific Ca^{2+}-dependent autocatalytic cleavage of an Asp-Pro peptide bond resulting in the release of the N-terminal segment of the polypeptide and its nonspecific covalent linkage to adjacent protein molecules through an Asp-Lys isopeptide bond. The cleavage of the Asp-Pro bond is catalyzed by the Ca^{2+}-dependent structural transition of a highly conserved SPM that along with multiple blocks of C-terminal RTX repeats remains located within the C-terminal portion of the cleaved polypeptide (Kuban et al., 2020; Matyska Liskova et al., 2016). The RTX repeats have been shown to fold in the presence of Ca^{2+} ions into a parallel β-roll structure that is primarily involved in the maintenance of protein stability or facilitating the protein secretion, and as such, does not exert any enzymatic or cytotoxic activity (Baumann, 2019; Goldsmith et al., 2021). Therefore, only the N-terminal segment of ApxIVA ($ApxIVA_{1–638}$), released through the autocatalytic cleavage of the Asp_{638}-Pro_{639} peptide bond, may harbor a potential toxic/effector function.

In this work, we demonstrated that $ApxIVA_{1–570}$, a truncated variant of the N-terminal segment of ApxIVA ($ApxIVA_{1–638}$), displays an antimicrobial activity. Notably, this activity exhibited a narrow target range, being directed only against the XL-1 Blue strain of *E. coli* (Fig. 6), suggesting that $ApxIVA_{1–570}$ is highly selective towards a specific group of Gram-negative bacteria. This observation nicely ties the functional data with the structural information of $ApxIVA_{1–570}$. Structural similarity searches revealed that the predicted $ApxIVA_{1–570}$ structure does not share any homology to other known protein structures but resembles the structures of colicin M-like bacteriocins, such as syringacin M (Grinter et al., 2012), pyocin M (Barreteau et al., 2012), pectocin M2 (Grinter et al., 2014) and colicin M (ColM) (Zeth et al., 2008). Colicins represent a diverse group of high molecular weight antimicrobial proteins (bacteriocins) that are produced by certain strains of *E. coli* to control and kill other strains of *E. coli* or related bacterial species within interspecies and intraspecies competition (Bosák et al., 2021; Cascales et al., 2007; Papadakos et al., 2012). Most of colicins exert their lethal effect either by the formation of a pore in the cytoplasmic membrane of the target cell, or by intracellular nuclease action on DNA, rRNA, or tRNA. In contrast, ColM is a unique colicin that exerts its lethal activity in the periplasm of target cells, where it inhibits peptidoglycan synthesis through the enzymatic degradation of undecaprenyl phosphate-linked peptidoglycan precursors (Chérier et al., 2021). In line with that, $ApxIVA_{1–570}$ can be excluded as a pore-forming bacteriocin, since no membrane activity of the recombinant $ApxIVA_{1–570}$ protein was recorded on planar lipid bilayer experiments (data not shown). Moreover, due to the absence of the C-terminal cytotoxic domain in the predicted $ApxIVA_{1–570}$ structure (Fig. 3A), $ApxIVA_{1–570}$ does not appear to exert any intracellular nuclease activity. Instead, $ApxIVA_{1–570}$ and ColM present compact structures with elongated shape consisting of α-helical N-terminal domain and C-terminal β-sheet structures. On the other hand, the $ApxIVA_{1–570}$ polypeptide is twice the size of the ColM polypeptide (570 vs. 271 residues) with no apparent sequence similarity

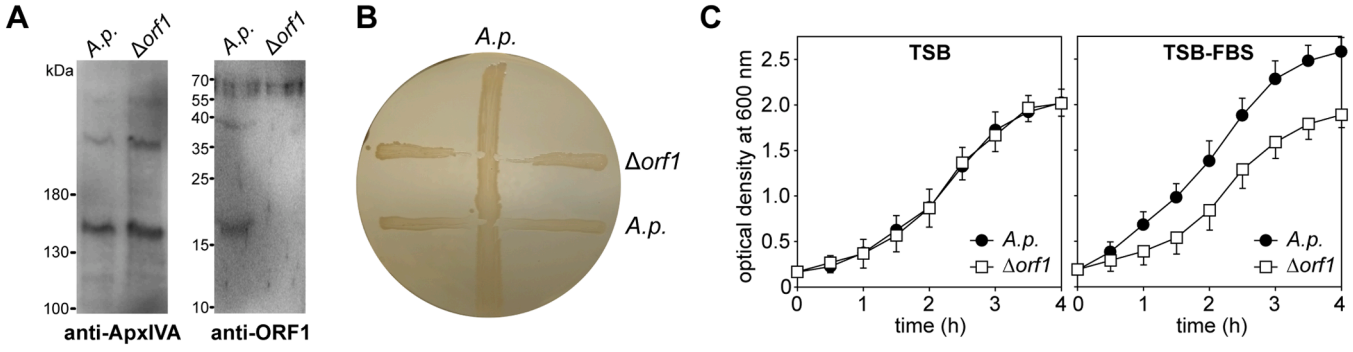

Fig. 7. ORF1 enhances the fitness of *A. pleuropneumoniae*. (A) Western blot analysis of ApxIVA (left panel) and ORF1 (right panel) production in the parental (*A. p.*) and mutant (Δ*orf1*) strains of *A. pleuropneumoniae*. The cells were cultivated at 37 °C in TSB-FBS medium and the protein samples from the culture supernatants and pelleted cells were separated on 5 % and 15 % SDS-PAGE gels, respectively. The separated proteins were transferred to a nitrocellulose membrane and probed with mouse polyclonal sera against ApxIVA and $ORF1_{23–157}$. (B) Cross-streak of the parental (*A.p.*) and the Δ*orf1* mutant strains of *A. pleuropneumoniae* against the parental *A. pleuropneumoniae* grown on TSB agar plates supplemented with 10 % FBS. (C) The growth curves of the parental and the Δ*orf1* mutant strains of *A. pleuropneumoniae* cultivated in TSB (left panel) and TSB-FBS (right panel) media. The bacterial growth was monitored by measurement of optical density at 600 nm. The error bars represent the mean ± SD from the three independent experiments.

between the proteins. However, both ApxIVA$_{1–570}$ and ColM structures form a linear patch of the surface-exposed negatively charged residues that are identically located at the interface between the α-helical N-terminal domain and the C-terminal β-sheet structures. Intriguingly, these residues (ColM$_{226–236}$) have been previously identified to be essential for binding and/or catalytic activity of ColM (Barreteau et al., 2010). Based on the structural and biochemical data, we conclude that ApxIVA$_{1–570}$ represents a bacteriocin with ColM-like properties, which equally to ColM, exerts its cytotoxic effect in the periplasm of bacterial cells.

This conclusion is further supported by the findings that the *orf1* gene product (ORF1), encoded upstream of the *apxIVA* gene in the same operon, functions as an immunity protein against ApxIVA. Immunity proteins are small high affinity protein antagonists that protect bacteriocin-producing cells. They protect them from auto-inhibition, as well as from the same bacteriocin, produced by neighboring cells (Cascales et al., 2007). For enzyme colicins, the products of the immunity gene are usually located downstream of the colicin-encoding genes and, along with the cognate colicins, form a stable complex neutralizing the catalytic activity of the colicin. The exception is the ColM immunity protein, Cmi (or ImM), which is located in the periplasm while anchored to the plasma membrane by an N-terminal transmembrane segment (Chérier et al., 2021). The anchor is not mandatory but increases the protective efficacy of Cmi against ColM (Gross and Braun, 1996). In line with that we demonstrated that ORF1 is produced as a cytosolic pre-protein that is exported to the periplasm by virtue of its N-terminal signal peptide using the general secretory (Sec) pathway (Fig. 4A). Additionally, the structure of the signal-less ORF1 (ORF1$_{23–157}$) appears to be similar with that of the soluble periplasmic domain of Cmi solved by X-ray crystallography (Gérard et al., 2011). In spite of sequence diversity, both ORF1$_{23–157}$ and Cmi structures share a common fold that is stabilized by an intramolecular disulfide bridge between two cysteine residues linking the N- and C-terminal regions of the protein (Fig. 4D). The disulfide bridge is thought to maintain the functional conformation of Cmi and essential for its activity (Gérard et al., 2011). Similarly, the elimination of the disulfide bridge in the ORF1 structure had detrimental impact on the stability of the ORF1$_{38–157}$ construct (Fig. 4B). The alignment of both the structural and functional data likely explain the phenotype of mutants lacking the *orf1* gene (Δ*orf1*). Yuan et al. (2011) reported that the deletion of the *orf1* gene lead to decreased virulence of *A. pleuropneumoniae* in pigs (Yuan et al., 2011). Considering that ApxIVA has a potential to harm the producer cells, the absence of ORF1 renders bacterial cells more susceptible to ApxIVA, which would result in decreased bacterial burden in pig lungs and ultimately virulence attenuation. This corresponds with our data showing that the Δ*orf1* mutant is not as competitive against the parental strain as the parental strain against itself, and its growth rate is decelerated under conditions promoting production of ApxIVA (Fig. 7B and Fig. 7C). Based on analogies with Cmi, it is likely that ORF1 functions as a periplasmic immunity protein that protects bacterial cells against the cytotoxic activity of ApxIVA. However, ORF1$_{23–157}$ does not form a stable complex with ApxIVA$_{1–570}$, as manifested by size exclusion chromatography (Supplementary Fig. S4A) and the inability of the recombinant ORF1$_{23–157}$ to inhibit the cytotoxic activity of ApxIVA$_{1–570}$ (Fig. 6). Likewise, no genuine interaction between Cmi and ColM has not been demonstrated yet indicating more specific condition(s) for neutralization of M-class bacteriocins (Chérier et al., 2021).

Bacteriocins are considered as a highly efficient means for eliminating competitor cells from the immediate environment of the producer cells. However, the production of bacteriocins is very costly and frequently accompanied with lysis of a particular fraction of the producer cells. Therefore, bacteriocin production is often tightly regulated to occur only under specific conditions, which probably (also) applies to ApxIVA and ORF1 proteins. Of importance, ApxIVA has been repeatedly reported to be expressed exclusively *in vivo* (in infected pigs) and not under *in vitro* conditions (Deslandes et al., 2010; Cho and Chae, 2001; Liu et al., 2009; Sheehan et al., 2003; Schaller et al., 1999). In contrast, the recent work has demonstrated that ApxIVA can be produced under *in vitro* conditions when *A. pleuropneumoniae* cells are cultured in medium supplemented with BD BBL™ IsoVitaleX™ Enrichment (Stancheva et al., 2022). IsoVitaleX is declared to be a chemically defined additive used for cultivating nutritionally fastidious microorganisms. Similarly, culturing *A. pleuropneumoniae* cultured in tryptic soy broth supplemented with 10 % fetal bovine serum (TSB-FBS) was shown to promote the production of ApxIVA into the culture medium (Fig. 5). In addition, TSB-FBS also induced the expression and production of ORF1. These findings suggest that both IsoVitaleX and FBS may contain a specific component (s) capable of promoting the transcription of genes within the *apxIVA* operon. However, the identity of this component remains unknown and requires further investigation.

FBS is the most commonly used medium supplement containing a natural mix of nutrients, growth factors, proteins and other substances that support cell proliferation in tissue cultures. Nevertheless, these substances are also integral components of a bulk plasma exudate that is transmitted outward across pseudostratified airway epithelial lining in response to microbial infection, and with its content of immunoglobulins, complement factors and more, can combat bacteria deposited on the mucosal surface (Persson, 2019). Hence, it is tempting to speculate that the colonization of the porcine respiratory tract with *A. pleuropneumoniae* is accompanied by plasma exudation, of which a yet unidentified component signals the expression of the genes in the *apxIV* operon (Fig. 8). This leads to a tightly controlled spatiotemporal production of the ORF1 and ApxIVA proteins during early stages of infection. The former is exported to the periplasm as an immunity protein, protecting the producer cell against the antimicrobial activity of the latter, which is recognized by the Type 1 secretion system and excreted into the extracellular space. Millimolar concentrations of calcium ions in mucosal fluid induce the Ca^{2+}-dependent autocatalytic cleavage of ApxIVA, releasing the N-terminal segment of ApxIVA (ApxIVA$_{1–638}$) from its C-terminal domain containing RTX repeats. Remarkably, the release of ApxIVA$_{1–638}$ appears to be essential for its antimicrobial activity to occur, as the deletion of SPM from ApxIVA resulted in a reduced virulence in pigs (Kuban et al., 2020). The released ApxIVA$_{1–638}$ is then free to diffuse in mucosal fluid and its antimicrobial activity can be employed to outcompete the host-associated microbial community or inhibit major microbial competitors. Hence, the ORF1-ApxIVA pair increases the fitness of *A. pleuropneumoniae* in competition with other microorganisms and can be considered as a microbiome-shaping tool that may promote the invasion of a microbial community by the pathogenic bacterial strain (García-Bayona and Comstock, 2018; Heilbronner et al., 2021).

4. Materials and methods

4.1. Antibodies and reagents

The suicide vector for allelic exchange on the *A. pleuropneumoniae* chromosome (pEMOC2) and the *Escherichia coli* β2155 (Δ*dapA*) strain were generously provided by Gerald F. Gerlach (Institute for Innovative Veterinary Diagnostics, Hannover, Germany). The *pJFFapxIVA1HisC* plasmid for expression of the full-length C-terminally His-tailed ApxIVA protein was kindly provided by Joachim Frey (Faculty of Veterinary Medicine, University of Bern, Switzerland).

4.2. Bacterial strains and growth conditions

Escherichia coli XL-1 Blue (Stratagene, USA) were grown at 37 °C on Luria-Bertani (LB) agar plates in the presence of appropriate antibiotics: kanamycin (30 μg/ml) or ampicillin (150 μg/ml). *E. coli* BL21 λ(DE3) were grown at 37 °C or 18 °C in the medium containing 20 g/l glycerol, 20 g/l yeast extract, 10 g/l KH_2PO_4, 30 g/l K_2HPO_4, 20 g/l NH_4Cl, 5 g/l Na_2SO_4 and 0.1 g/l thiamine. For detection of alkaline phosphatase

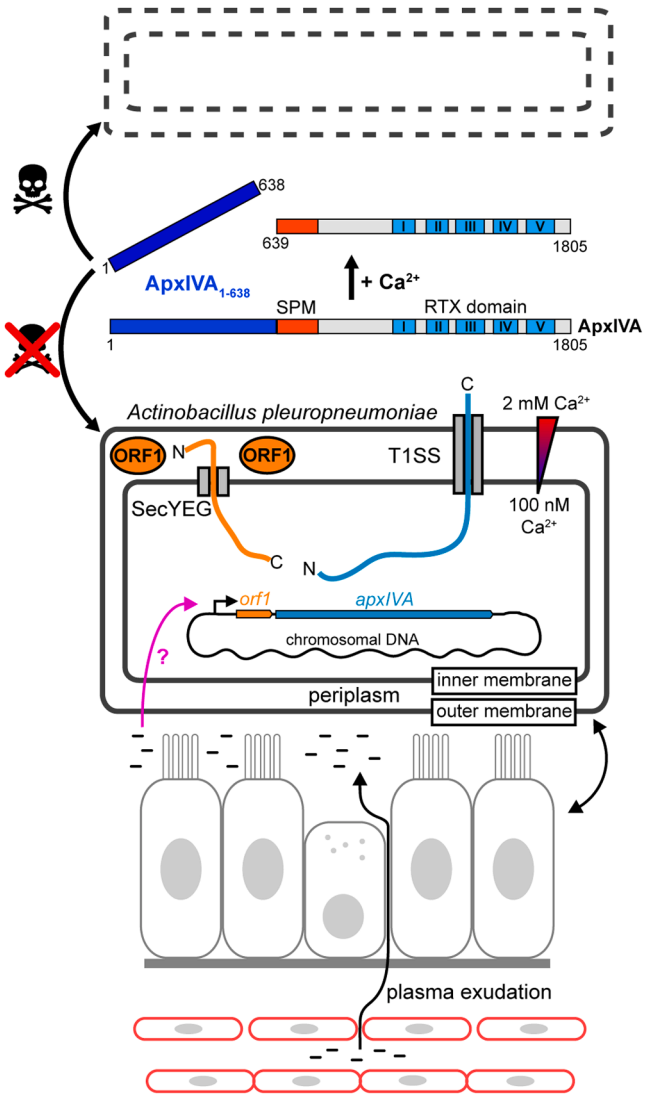

Fig. 8. Proposed model of the ORF1 and ApxIVA action. The interaction of the Gram-negative bacterium *Actinobacillus pleuropneumoniae* with the airway mucosal surface is accompanied by plasma exudation, which contains an as-yet unidentified component that promotes the transcription of the *orf1* and *apxIVA* genes within the *apxIV* operon. The *orf1* gene product (ORF1) is exported to the periplasm via its N-terminal signal peptide through the general secretory pathway (SecYEG) and protects bacterial cells against the antimicrobial activity of the N-terminal domain of the ApxIVA protein ($ApxIVA_{1–638}$). This N-terminal domain is released from the full-length ApxIVA after translocation by the Type 1 Secretion System (T1SS) into the calcium-rich external environment, where it is processed by Ca^{2+}-dependent autocatalytic cleavage of the Asp_{638}-Pro_{639} peptide bond mediated by the SPM.

(PhoA) activity, LB agars were supplemented with 0.16 mg/ml 5-bromo-4-chloro-3-indolyl-phosphate and 0.32 mg/ml nitro blue tetrazolium (BCIP/NBT Color Development Substrate, Promega). *Actinobacillus pleuropneumoniae* 4074 (serovar 1) was obtained from The Collection of Animal Pathogenic Microorganisms (https://capm.vri.cz/en) under the catalogue number CAPM 5869 T. The *A. pleuropneumoniae* cells were grown at 37 °C in grown in a 5 % CO_2 atmosphere at 37 °C in a Bacto tryptic soy broth (TSB; BD Biosciences, USA) supplemented with 10 μg/ml β-nicotinamide adenine dinucleotide (β-NAD; Sigma).

4.3. Cell cultures, growth conditions and handling of cells

Newborn pig tracheal (NPTr) cells were kindly provided by Francois Meurens (Nantes-Atlantic National College of Veterinary Medicine, Food Science and Engineering, Nantes, France). The NPTr cells were cultured in DMEM (Sigma) supplemented with 10 % fetal bovine serum (FBS; Life technologies) and antibiotic/antimycotic solution (0.1 mg/ml streptomycin, 100 U/ml penicillin and 0.25 μg/ml amphotericin [Sigma]) at 37 °C in a 5 % CO_2 atmosphere. Porcine alveolar macrophages (PAMs) were collected by bronchoalveolar lavage from 12-weeks-old pigs as described previously (Kavanová et al., 2017). In brief, healthy pigs were euthanized with the intravenous injection of the anesthetic T61 (Intervet International, Netherlands) based on body weight according to the manufacturer's recommendations (1 ml/10 kg of body weight) and necropsied. The trachea and lungs were immediately removed, and the lungs were flushed with DPBS (Lonza). PAMs were pelleted by centrifugation of the bronchoalveolar lavage fluid at 300 g for 10 min at 25 °C and maintained in DMEM (Sigma) supplemented with 10 % FBS (Life technologies) at 37 °C in a 5 % CO_2 atmosphere.

4.4. Cell fractionation

Cell fractionation of *A. pleuropneumoniae* cells was performed by cold osmotic shock followed by freeze–thaw cycle as described previously (Malherbe et al., 2019). In brief, the *A. pleuropneumoniae* cells were grown in 20 ml of TSB medium supplemented with 10 μg/ml β-NAD and 10 % FBS (TSB-FBS) until an optical density at 600 nm of 3, and centrifuged at 5,000 *g* for 15 min at 4 °C. The supernatant was carefully removed and referred as the culture supernatant fraction. The pelleted cells were washed in phosphate buffer saline (PBS) solution, resuspended in 500 μl of 100 mM Tris-HCl (pH 8.0), 500 mM sucrose, 5 mM EDTA and diluted with 500 μl distilled water before adding 40 μl lysozyme (2 mg/ml). After 5-min incubation followed by the addition of 20 μl $MgSO_4$ (1 M), the cells were centrifuged at 20,000 g for 3 min at 4 °C and the supernatant was transferred into a fresh tube as the periplasmic fraction. The pelleted spheroplasts were lyzed by freeze–thaw cycle and referred as the cytoplasmic fraction.

4.5. Plasmid construction

The pET28b-ApxIC and pET28b-ApxIIC vectors were constructed by ligating the *Nco*I/*Hin*dIII-cleaved fragment of pET28b with the *Nco*I/*Hin*dIII-digested PCR products. These PCR products were amplified from the genomic DNA of *A. pleuropneumoniae* 4074 using primers P1 and P2 for ApxIC, and primers P3 and P4 for ApxIIC (see primer sequences in Table S1). The pET28b-ApxIIIC vector was constructed by cloning the synthetic DNA sequence encoding ApxIIIC (GeneArt, Thermo Fisher Scientific) into the *Nco*I/*Hin*dIII-cleaved fragment of pET28b using the Gibson assembly strategy. The pET22b-$ORF1_{23–157}$ and pET22b-$ORF1_{38–157}$ vectors were prepared by ligating the *Nco*I/*Xho*I-digested pET22b with the *Nco*I/*Xho*I-digested PCR products. These PCR products were amplified from the genomic DNA of *A. pleuropneumoniae* 4074 using primers P5 and P6 for $ORF1_{23–157}$, and primers P7 and P8 for $ORF1_{38–157}$. The pET28b-dHis-TEV-$ApxIVA_{1–570}$ vector was constructed by ligation of the modified, *Hin*dIII/*Xho*I-digested pET28b (encoding the N-terminal double His Tag) with the *Hin*dIII/*Xho*I-digested PCR product amplified from genomic DNA of *A. pleuropneumoniae* 4074 using the P9 and P10 primers. The pTZ19R-$PhoA_{1–471}$ and pTZ19R-$PhoA_{23–471}$ vectors were prepared by Gibson assembly of the *Hin*dIII/*Eco*RI-digested pTZ19R vector and PCR products amplified from genomic DNA of *Escherichia coli* 536 using the P11 and P12 primers ($PhoA_{1–471}$), and the P11 and P13 primers ($PhoA_{23–471}$). The pTZ19R- $ORF1_{1–25}$-$PhoA_{23–471}$ vector was constructed using Gibson assembly, combining the *Hin*dIII/*Eco*RI-digested pTZ19R vector with two DNA fragments. The first fragment, encoding the signal peptide of ORF1 ($ORF1_{1–25}$), was amplified by PCR using primers P14 and P15. The second fragment, encoding the signal-less alkaline phosphatase ($PhoA_{23–471}$), was amplified using primers P16 and P17. For the construction of the pEMOC2-ΔORF1 allelic

exchange vector, two DNA fragments corresponding to the 5′ and 3′ flanking regions of the in-frame deletion were amplified from the genomic DNA of *A. pleuropneumoniae* 4074 using primer pairs P18/P19 and P20/P21 and cloned into the *Not*I/*Apa*I-digested pEMOC2 vector using the Gibson assembly strategy. All constructs were confirmed by DNA sequence analysis with an ABI Prism 3130XL analyzer (Applied Biosystems, USA) using a BigDye Terminator cycle sequencing kit.

4.6. Construction of the orf1 deletion mutant in A. pleuropneumoniae

In-frame deletion of the orf1 gene was performed on chromosome of *Actinobacillus pleuropneumoniae* 4074 by homologous recombination using a pEMOC2 allelic exchange vector as previously described (Kuban et al., 2020). Briefly, *A. pleuropneumoniae* cells grown in a 5 % CO_2 atmosphere at 37 °C on Bacto tryptic soy broth agar (BD Biosciences) supplemented with 10 μg/ml β-NAD (NAD; Sigma) were mated on fresh agar plates supplemented with 10 μg/ml NAD, 1 mM diaminopimelic acid (DAPA; Sigma), and 10 mM $MgSO_4$ with *E. coli* β2155 grown on LB agar supplemented with 1 mM DAPA and 25 μg/ml chloramphenicol (Cm) before being transformed with the pEMOC2-ΔORF1 plasmid construct. After 4 h at 37 °C, the *A. pleuropneumoniae* transconjugants were selected on Bacto tryptic soy broth agar plates supplemented with 10 μg/ml NAD and 5 μg/ml chloramphenicol and incubated in 5 % CO_2 for 24 h at 37 °C. For sucrose counterselection, the single Cm^r colonies were inoculated into salt-free LB broth supplemented with 10 % sucrose, 10 % horse serum, and 10 μg/ml NAD, incubated with shaking at 37 °C for 2 h, and plated on salt-free LB broth supplemented with 10 % sucrose, 10 % horse serum, and 10 μg/ml NAD. Sucrose-resistant colonies were screened for the absence of the *orf1* nucleotide sequence by a colony PCR.

4.7. Expression, purification and handling of proteins

The ApxIVA, $ApxIVA_{1–570}$, ORF1 and ApxIA proteins were expressed as recombinant C-terminally His-tagged proteins in *E. coli* BL21 λ(DE3) cells. The cells were transformed with appropriate plasmid construct, grown at 37 °C and induced with 1 mM isopropyl 1-thio-β-D-galactopyranoside (IPTG, Alexis, Switzerland) when the optical density at 600 nm (OD_{600}) reached 0.6. The cells were then cultivated at 37 °C for additional 4 h, except for ORF1, which was cultured at 18 °C for 16 h.

The ApxIVA protein was purified under denaturing conditions from insoluble inclusion bodies obtained by centrifuging the bacterial cell lysate at 20,000 g at 4 °C for 30 minutes following disruption of bacterial cells using ultrasonic processing (Misonix S-4000, Qsonica, USA) on ice. The pelleted inclusion bodies were solubilized in buffer containing 50 mM Tris-HCl (pH 8.0) and 8 M urea (TU buffer), and the urea extract was clarified by centrifugation at 20,000 g at 4 °C for 30 min. The supernatant was loaded on Ni-Sepharose affinity column (GE Healthcare, USA) equilibrated with TU buffer. After loading, the column was washed extensively with TU buffer and ApxIVA was eluted from the column with TU buffer containing 100 mM imidazole. These imidazole fractions were collected and loaded on Q-Sepharose anion-exchange column (GE Healthcare) equilibrated with TU buffer supplemented with 100 mM NaCl (TUN). After washing the column with TUN, the purified ApxIVA protein was eluted with TU buffer containing 250 mM NaCl. Renaturation of ApxIVA was performed by a rapid dilution of the urea-unfolded protein into prewarmed cell culture medium directly in the presence of target cells, as described previously (Basler et al., 2006). The ApxIVA samples were prediluted from concentrated stocks to 100 times the final indicated concentration using TU buffer. Before addition to cells, the ApxIVA solutions were first rapidly diluted 25 times in prewarmed medium, to reduce the urea concentration to 0.32 M, and 50-μl aliquots of the diluted toxin samples were immediately admixed with 150 μl of medium covering the cells. This yielded the indicated toxin concentrations and a final urea concentration of 80 mM. Appropriate blanks containing identical amounts of cells incubated with 80 mM urea in medium were systematically scored in all activity assays, and no effect whatsoever of the 80 mM urea concentration on cell viability and/or enzymatic activities was observed.

The $ApxIVA_{1–570}$ protein was purified under denaturing conditions from 8 M urea extract of inclusion bodies prepared as described above. In brief, the urea extract was loaded on Q-Sepharose anion-exchange column (GE Healthcare) equilibrated with TUN buffer. After loading, the column was extensively washed with TUN buffer and $ApxIVA_{1–570}$ was eluted from the column with TU buffer supplemented with 200 mM NaCl. The eluted fractions were collected and loaded on Ni-Sepharose affinity column (GE Healthcare) equilibrated with TU buffer. The column was extensively washed with TU buffer containing 10 mM imidazole and the purified $ApxIVA_{1–570}$ was eluted from the column with TU buffer containing 100 mM imidazole. Refolding of $ApxIVA_{1–570}$ into native conformation was performed by a rapid dilution of the urea-unfolded protein into a buffer containing 20 mM Hepes (pH 7.4), 135 mM NaCl and 5 mM KCl. The refolded protein was concentrated by ultrafiltration using Amicon Stirred Cell equipped with 10 kDa NMWL Ultracel ultrafiltration discs (Merck Millipore, USA). The concentrated protein was loaded a Superdex 200 Increase 10/300 size-exclusion column connected to an AKTA Pure chromatography system (GE Healthcare). The column was equilibrated with 20 mM Tris-HCl (pH 7.4) and 150 mM NaCl and run at a flow rate of 0.5 ml/min. Chromatograms were recorded at 280 nm. The fractions of monomeric $ApxIVA_{1–570}$ were collected and stored at 4 °C for further use.

The $ORF1_{23–157}$ protein was recovered in the periplasmic space of bacterial cells and purified from the cell lysate following the disintegration of bacterial cells by a high-pressure cell disruptor (French press G-M, Glen-Mills, USA) at 15000 psi. Unbroken cells were removed by centrifugation at 3000 g for 10 min and the cell lyzate was clarified by centrifugation at 20,000 g at 4 °C for 30 min. The supernatant was loaded on Ni-Sepharose affinity column (GE Healthcare) equilibrated with PBS. After loading, the column was extensively washed with PBS containing 25 mM imidazole and $ORF1_{23–157}$ was eluted from the column with PBS containing 200 mM imidazole. The collected fractions were concentrated by ultrafiltration using Amicon Stirred Cell equipped with 3 kDa NMWL Ultracel ultrafiltration discs (Merck Millipore, USA). The concentrated protein was loaded a Superdex 75 Increase 10/300 size-exclusion column connected to an AKTA Pure chromatography system (GE Healthcare). The column was equilibrated with PBS and run at a flow rate of 0.5 ml/min. The fractions of monomeric $ORF1_{23–157}$ were collected and stored at 4 °C for further use.

ApxIA was expressed in the presence of ApxIA-activating lysin acyltransferase (ApxIC) and purified as described previously (Masin et al., 2013).

The purity of protein samples was monitored by SDS-PAGE. Protein concentrations were determined by Bradford assay (Bio-Rad) using bovine serum albumin (Sigma) as a standard.

4.8. Cytotoxicity assays

Cytotoxic activities of proteins toward primary porcine alveolar macrophages (PAMs) and newborn pig tracheal (NPTr) cells were assessed by measuring cell membrane integrity using the CellTox Green Cytotoxicity Assay (G8743, Promega), as described previously (Malcova et al., 2021). Briefly, aliquots of PAMs (5×10^4) and NPTr (2×10^4) cells were seeded into a 96-well plate in DMEM supplemented with 10 % FBS and cultured overnight at 37 °C in a 5 % CO_2 atmosphere. Prior to the experiment, the medium was replaced with the prewarmed DMEM medium (150 μl) supplemented with different concentrations of proteins and the CellTox Green probe (500 × dilution). Changes in cell membrane integrity were monitored by measuring fluorescence intensity at an excitation wavelength of 490 nm and an emission wavelength of 520 nm, using a Spark multimode microplate reader (Tecan, Switzerland). The measurements were taken for 8 hours at 10-minute intervals, maintaining cells at 37 °C in a 5 % CO_2 atmosphere.

4.9. Hemolytic activity on sheep erythrocytes

The pore-forming activity of proteins was assessed by measuring hemoglobin release over time following incubation with sheep erythrocytes (LabMediaServis, Czech Republic), as described previously (Masin et al., 2013). In brief, erythrocytes (5×10^8 cells/ml) suspended in HBSS buffer were incubated with 1 μg/ml of protein at 37 °C. At indicated time points, aliquots of the suspension were centrifuged at 8000 g for 5 min, and the hemoglobin released into the supernatant was quantified by measuring absorbance at 540 nm.

4.10. Spot-on-lawn assay

The overnight culture of *E. coli* XL-1 Blue cells ($OD_{600\ nm}$~1.0) was diluted tenfold with LB medium and 50 μl of the suspension plated on LB agar plate. Tenfold serial dilutions of purified proteins were spotted on the dry agar (5 μl/spot) and incubate overnight at 30 °C.

4.11. Cross-streak assay

The exponentially grown culture of *A. pleuropneumoniae* 4074 was streaked vertically on the TSB agar plates supplemented with 10 % FBS and 10 μg/ml β-nicotinamide adenine dinucleotide. After overnight incubation at 37 °C, the wild-type and the Δ*orf1* strains were streaked, horizontally, from the edge of the plate to the pre-grown wild-type streak and incubated overnight at 37 °C.

4.12. Animal experiments

The animal experiments were carried out according to the guidelines for the animal care Act No. 246/1992 Coll. of the Czech Republic. The experiments with pigs were approved by the Animal Welfare Commission of the Ministry of Agriculture of the Czech Republic (Approval protocol No. MZe 1487) and conducted in the accredited barrier-type stables at the Veterinary Research Institute (Brno, Czech Republic). Four-weeks-old pigs were purchased from a porcine reproductive and respiratory syndrome virus- and *A. pleuropneumoniae*-free herd (Bioprodukt Knapovec, Czech Republic) as tested by serological reaction in enzyme-linked immunosorbent assays (ELISA). Pigs were regularly monitored throughout the housing period at least three times per day.

The mice experiments were approved by the Animal Welfare Committee of the Institute of Molecular Genetics of the Czech Academy of Sciences (Approval protocol 19/2020) and conducted in the animal house of the Institute of Molecular Genetics of the Czech Academy of Sciences (Prague, Czech Republic).

4.13. Preparation of mouse polyclonal sera

Five-week-old female BALB/cByJ mice (Charles River, France) were immunized by intraperitoneal injection of the ApxIVA and $ORF1_{23–157}$ proteins (30 μg per mouse) adjuvanted with aluminum hydroxide (SevaPharma, Czech Republic). Control mice were vaccinated with the adjuvanted PBS. Mice received three doses of the vaccines in two-weeks interval and one week after the third immunization blood was collected from anesthetized animals (i.p. injection of 80 mg/kg ketamine and 8 mg/kg xylazine) by retroorbital puncture method. Sera were recovered from the supernatant after centrifugation of clogged blood at 5000 g for 10 min at 8 °C and stored at −20 °C.

4.14. Mass spectrometry

Acylation status of ApxIVA proteins was analyzed by LC-MS/MS approach. The ApxIVA proteins were dissolved in 50 mM ammonium bicarbonate (pH 8.3) to reach 4 M concentration of urea and digested with trypsin (Promega, USA) at a trypsin/protein ratio of 1:50 for 6 h at 30 °C. The second portion of trypsin was added to a final ratio of trypsin/protein of 1:25, and the reaction was carried out for another 6 h at 30 °C. The concentration of the resulting peptides was adjusted by 0.1 % trifluoroacetic acid (TFA) to 0.1 mg/ml, and 5 μl of the samples were injected into the LC-MS/MS system. The separation of peptides was performed using a Zorbax C18 SB-300 (0.1 ×2 mm) desalting column (Shimadzu, Japan) in 0.1 % formic acid (FA) at a flow rate of 40 μl/min, and a Zorbax C18 SB-300 (0.2 ×150 mm) separation column ((Shimadzu, Japan) at a flow rate of 10 μl/min connected to an Agilent 1200 chromatography system (Agilent Technologies, USA). The peptides were eluted using a water/acetonitrile (Merck, Germany) gradient: 0–1 min, 0.2 % FA in 5 % acetonitrile; 5 min, 0.2 % FA in 10 % acetonitrile; 35 min, 0.2 % FA in 50 % acetonitrile; 40 min, 0.2 % FA in 95 % acetonitrile; 45 min, 0.2 % FA in 95 % acetonitrile. A capillary column was directly connected to a mass analyzer. The MS/MS analysis was performed on a commercial solariX XR FTMS instrument equipped with a 15 Tesla superconducting magnet and a Dual II ESI/MALDI ion source (Bruker Daltonics, Germany). Mass spectra of the samples were obtained in the positive ion mode within an *m/z* range of 150–2000. The accumulation time was set at 0.2 s, LC acquisition was 45 min with a 5-min delay, and one spectrum consisted of accumulation of four experiments. The instrument was operating in MS/MS data dependent acquisition mode. MS data were processed using the SNAP algorithm v2.0 of the DataAnalysis 4.4 software package (Bruker Daltonics, USA) generating a list of monoisotopic masses from deconvoluted spectra. The parameters were set as follows: export *m/z* range of 150–2000, maximum charge state of 8, signal/noise threshold of 0.75, and absolute intensity threshold 5×10^5. The extracted datasets were searched against the FASTA of the ApxIVA protein sequence (Uniprot: A3N106) using Linx software (https://scicrunch.org/resolver/RRID:SCR_018657). The Linx parameters were set for fully tryptic restriction with a maximum of three missed cleavages and variable modification for methionine oxidation. The mass error threshold was set to ± 2 ppm and MS/MS fragmentation spectra of assigned peptides were verified using DataAnalysis 4.4.

Characterization of disulfide bridges in ORF1 proteins was analyzed by MALDI-TOF technology. The ORF1 proteins were digested with trypsin in 50 mM ammonium bicarbonate (pH 8.3) buffer at a trypsin/protein ratio of 1:50 for 18 h at 37 °C. Resulting peptides were desalted by protein MacroTrap (Optimize Technologies, USA), eluted with 100 μl of acetonitrile and dried via vacuum centrifugation. Sample was reswelled in 10 μl of 3 % acetonitrile, 0.1 % TFA and two 0.5 μl aliquots of the ORF1 tryptic digests were spotted on the MALDI plate. One of the samples underwent on-target reduction using 0.5 μl of 50 mM dithiothreitol while the other one stayed untreated. After 20 min at room temperature, both samples were covered by 0.5 μl α-Cyano-4-hydroxycinnamic acid. Dried spots were analyzed by MALDI-TOF MS using an Autoflex III (Bruker Daltonics, USA) instrument with mass spectra acquisition in the positive reflection mode within a scan range of 300–4000 Da. Results were processed using DataAnalysis 4.4 (Bruker Daltonics).

4.15. Circular dichroism (CD) spectroscopy

The far-UV CD spectra were recorded at 25 °C on a Chirascan-plus spectrometer (Applied Photophysics, USA) in a rectangular quartz Suprasil cells of 1-mm path length (110-QS, Hellma, Germany). Protein samples (100 μg/ml) were diluted in 5 mM Tris-HCl (pH 7.4), 50 mM NaCl and measured for wavelengths from 200 to 260 nm at 20 °C. Two spectra accumulations with standard instrument sensitivity and scanning speed of 1 nm/s were acquired. The spectra of the buffers was subtracted from the protein spectra and mean molar ellipticity (Θ) was expressed in degrees square centimeter per decimole [$deg.cm^{-2}.dmol^{-1}$].

4.16. SDS-PAGE and western blotting

The proteins were separated by SDS-polyacrylamide gel

electrophoresis (SDS-PAGE) and transferred to a nitrocellulose membrane (Immobilon-NC, GE Healthcare) using a Hoefer SemiPhor semi-dry transfer unit (Amersham, USA). The membranes were blocked with 5 % nonfat milk in 50 mM Tris-HCl (pH 8.0), 150 mM NaCl, 0.05 % Tween-20 (TNT buffer) and incubated with mouse polyclonal sera diluted at 5000 × (ORF1) and 20,000 × (ApxIVA) in TNT buffer. The chemiluminescent signal was developed on G:Box Chemi XRQ gel doc system (Syngene, USA) using a SuperSignal West Femto substrate (Thermo Fisher Scientific, USA) after incubation of the membrane with a horseradish peroxidase-conjugated goat anti-mouse secondary antibody (GE Healthcare).

CRediT authorship contribution statement

Ludmila Brazdilova: Methodology, Investigation, Formal analysis, Data curation. **Monika Cizkova:** Methodology, Investigation, Formal analysis, Data curation. **Ladislav Bumba:** Writing – review & editing, Writing – original draft, Visualization, Investigation, Data curation, Conceptualization. **Jana Holubova:** Methodology, Investigation, Formal analysis, Data curation. **Ondrej Stanek:** Methodology, Investigation, Formal analysis, Data curation. **David Jurnecka:** Methodology, Investigation, Formal analysis, Data curation. **Eva Slivenecka:** Methodology, Investigation, Formal analysis, Data curation.

Acknowledgement

This work was supported by the Ministry of Education, Youth and Sports of the Czech Republic (MEYS-CR) projects Talking microbes - understanding microbial interactions within One Health framework (CZ.02.01.01/00/22_008/0004597) and National Institute of Virology and Bacteriology (Programme EXCELES, ID Project No. LX22NPO5103) - Funded by the European Union - Next Generation EU. The research infrastructure projects LM2023053 (*EATRIS-CZ*) and LM2023042 (*CIISB*) of the MEYS of the Czech Republic are also acknowledged. Computational resources were provided by the e-INFRA CZ project (ID:90254), supported by the MEYS-CR. We thank Martin Foldyna and Katerina Nedbalcova (Veterinary Research Institute, Brno, Czech Republic) for providing primary porcine alveolar macrophages. Technical help of Iva Marsikova and Oliva Branna is also gratefully acknowledged.

Appendix A. Supporting information

Supplementary data associated with this article can be found in the online version at doi:10.1016/j.micres.2024.128043.

Data Availability

The mass spectrometry proteomics data have been deposited to the ProteomeXchange Consortium via the PRIDE partner repository with the dataset identifier PXD058195 and accessible at https://www.ebi.ac.uk/pride/. All data will be made available on request.

References

Abramson, J., Adler, J., Dunger, J., Evans, R., Green, T., Pritzel, A., Ronneberger, O., Willmore, L., Ballard, A.J., Bambrick, J., et al., 2024. Accurate structure prediction of biomolecular interactions with AlphaFold 3. Nature 630, 493–500.

Baltes, N., Gerlach, G.F., 2004. Identification of genes transcribed by Actinobacillus pleuropneumoniae in necrotic porcine lung tissue by using selective capture of transcribed sequences. Infect. Immun. 72, 6711–6716.

Barreteau, H., Bouhss, A., Gérard, F., Duché, D., Boussaid, B., Blanot, D., Lloubès, R., Mengin-Lecreulx, D., Touzé, T., 2010. Deciphering the catalytic domain of colicin M, a peptidoglycan lipid II-degrading enzyme. J. Biol. Chem. 285, 12378–12389.

Barreteau, H., Tiouajni, M., Graille, M., Josseaume, N., Bouhss, A., Patin, D., Blanot, D., Fourgeaud, M., Mainardi, J.L., Arthur, M., et al., 2012. Functional and structural characterization of PaeM, a colicin M-like bacteriocin produced by Pseudomonas aeruginosa. J. Biol. Chem. 287, 37395–37405.

Basler, M., Masin, J., Osicka, R., Sebo, P., 2006. Pore-forming and enzymatic activities of Bordetella pertussis adenylate cyclase toxin synergize in promoting lysis of monocytes. Infect. Immun. 74, 2207–2214.

Baumann, U., 2019. Structure-Function Relationships of the Repeat Domains of RTX Toxins. Toxins 11, E657.

Baumann, U., Wu, S., Flaherty, K.M., McKay, D.B., 1993. Three-dimensional structure of the alkaline protease of Pseudomonas aeruginosa: a two-domain protein with a calcium binding parallel beta roll motif. EMBO J. 12, 3357–3364.

Benz, R., 2016. Channel formation by RTX-toxins of pathogenic bacteria: Basis of their biological activity. Biochim Biophys. Acta 1858, 526–537.

Bode, W., Engh, R., Musil, D., Thiele, U., Huber, R., Karshikov, A., Brzin, J., Kos, J., Turk, V., 1988. The 2.0 A X-ray crystal structure of chicken egg white cystatin and its possible mode of interaction with cysteine proteinases. EMBO J. 7, 2593–2599.

Bosák, J., Hrala, M., Micenková, L., Šmajs, D., 2021. Non-antibiotic antibacterial peptides and proteins of Escherichia coli: efficacy and potency of bacteriocins. Expert Rev. anti-Infect. Ther. 19, 309–322.

Bosse, J.T., Janson, H., Sheehan, B.J., Beddek, A.J., Rycroft, A.N., Kroll, J.S., Langford, P. R., 2002. Actinobacillus pleuropneumoniae: pathobiology and pathogenesis of infection. Microbes Infect. 4, 225–235.

Bumba, L., Masin, J., Macek, P., Wald, T., Motlova, L., Bibova, I., Klimova, N., Bednarova, L., Veverka, V., Kachala, M., et al., 2016. Calcium-Driven Folding of RTX Domain beta-Rolls Ratchets Translocation of RTX Proteins through Type I Secretion Ducts. Mol. Cell 62, 47–62.

Cascales, E., Buchanan, S.K., Duché, D., Kleanthous, C., Lloubès, R., Postle, K., Riley, M., Slatin, S., Cavard, D., 2007. Colicin biology. Microbiol Mol. Biol. Rev. 71, 158–229.

Chérier, D., Patin, D., Blanot, D., Touzé, T., Barreteau, H., 2021. The Biology of Colicin M and Its Orthologs. Antibiot. (Basel) 10.

Chiers, K., De Waele, T., Pasmans, F., Ducatelle, R., Haesebrouck, F., 2010. Virulence factors of Actinobacillus pleuropneumoniae involved in colonization, persistence and induction of lesions in its porcine host. Vet. Res. 41, 65.

Cho, W.S., Chae, C., 2001. Expression of the apxIV gene in pigs naturally infected with Actinobacillus pleuropneumoniae. J. Comp. Pathol. 125, 34–40.

Deslandes, V., Denicourt, M., Girard, C., Harel, J., Nash, J.H., Jacques, M., 2010. Transcriptional profiling of Actinobacillus pleuropneumoniae during the acute phase of a natural infection in pigs. BMC Genom. 11, 98.

Domínguez, D.C., Guragain, M., Patrauchan, M., 2015. Calcium binding proteins and calcium signaling in prokaryotes. Cell Calcium 57, 151–165.

Dreyfus, A., Schaller, A., Nivollet, S., Segers, R.P., Kobisch, M., Mieli, L., Soerensen, V., Hussy, D., Miserez, R., Zimmermann, W., et al., 2004. Use of recombinant ApxIV in serodiagnosis of Actinobacillus pleuropneumoniae infections, development and prevalidation of the ApxIV ELISA. Vet. Microbiol 99, 227–238.

Frey, J., 2019. RTX Toxins of Animal Pathogens and Their Role as Antigens in Vaccines and Diagnostics. Toxins (Basel) 11.

Frey, J., Kuhnert, P., 2002. RTX toxins in Pasteurellaceae. Int. J. Med. Microbiol.: IJMM 292, 149–158.

García-Bayona, L., Comstock, L.E., 2018. Bacterial antagonism in host-associated microbial communities. Science 361, eaat2456.

Gavin, H.E., Satchell, K.J., 2015. MARTX toxins as effector delivery platforms. Pathog. Dis. *73*, ftv092.

Gérard, F., Brooks, M.A., Barreteau, H., Touzé, T., Graille, M., Bouhss, A., Blanot, D., van Tilbeurgh, H., Mengin-Lecreulx, D., 2011. X-ray structure and site-directed mutagenesis analysis of the Escherichia coli colicin M immunity protein. J. Bacteriol. 193, 205–214.

Goldsmith, J.A., DiVenere, A.M., Maynard, J.A., McLellan, J.S., 2021. Structural basis for antibody binding to adenylate cyclase toxin reveals RTX linkers as neutralization-sensitive epitopes. PLoS Pathog. 17, e1009920.

Gottschalk, M., 2015. The challenge of detecting herds sub-clinically infected with Actinobacillus pleuropneumoniae. Vet. J. 206, 30–38.

Grinter, R., Roszak, A.W., Cogdell, R.J., Milner, J.J., Walker, D., 2012. The crystal structure of the lipid II-degrading bacteriocin syringacin M suggests unexpected evolutionary relationships between colicin M-like bacteriocins. J. Biol. Chem. 287, 38876–38888.

Grinter, R., Josts, I., Zeth, K., Roszak, A.W., McCaughey, L.C., Cogdell, R.J., Milner, J.J., Kelly, S.M., Byron, O., Walker, D., 2014. Structure of the atypical bacteriocin pectocin M2 implies a novel mechanism of protein uptake. Mol. Microbiol. 93, 234–246.

Gross, P., Braun, V., 1996. Colicin M is inactivated during import by its immunity protein. Mol. Gen. Genet 251, 388–396.

Guo, S., Vance, T.D.R., Stevens, C.A., Voets, I.K., Davies, P.L., 2019. RTX Adhesins are Key Bacterial Surface Megaproteins in the Formation of Biofilms. Trends Microbiol. 27, 470.

Heilbronner, S., Krismer, B., Brötz-Oesterhelt, H., Peschel, A., 2021. The microbiome-shaping roles of bacteriocins. Nat. Rev. Microbiol. 19, 726–739.

Hoffman, C.S., Wright, A., 1985. Fusions of secreted proteins to alkaline phosphatase: an approach for studying protein secretion. Proc. Natl. Acad. Sci. USA 82, 5107–5111.

Holm, L., Laiho, A., Törönen, P., Salgado, M., 2023. DALI shines a light on remote homologs: One hundred discoveries. Protein Sci. 32, e4519.

Käll, L., Krogh, A., Sonnhammer, E.L., 2004. A combined transmembrane topology and signal peptide prediction method. J. Mol. Biol. 338, 1027–1036.

Kavanová, L., Matiašková, K., Levá, L., Štěpánová, H., Nedbalcová, K., Matiašovic, J., Faldyna, M., Salát, J., 2017. Concurrent infection with porcine reproductive and respiratory syndrome virus and Haemophilus parasuis in two types of porcine macrophages: apoptosis, production of ROS and formation of multinucleated giant cells. Vet. Res. 48, 28.

Kuban, V., Macek, P., Hritz, J., Nechvatalova, K., Nedbalcova, K., Faldyna, M., Sebo, P., Zidek, L., Bumba, L., 2020. Structural Basis of Ca(2+)-Dependent Self-Processing Activity of Repeat-in-Toxin Proteins. mBio 11.
Kuroda, T., Kubori, T., Thanh Bui, X., Hyakutake, A., Uchida, Y., Imada, K., Nagai, H., 2015. Molecular and structural analysis of Legionella DotI gives insights into an inner membrane complex essential for type IV secretion. Sci. Rep. 5, 10912.
Linhartova, I., Bumba, L., Masin, J., Basler, M., Osicka, R., Kamanova, J., Prochazkova, K., Adkins, I., Hejnova-Holubova, J., Sadilkova, L., et al., 2010. RTX proteins: a highly diverse family secreted by a common mechanism. FEMS Microbiol Rev. 34, 1076–1112.
Liu, J., Chen, X., Tan, C., Guo, Y., Chen, Y., Fu, S., Bei, W., Chen, H., 2009. In vivo induced RTX toxin ApxIVA is essential for the full virulence of Actinobacillus pleuropneumoniae. Vet. Microbiol 137, 282–289.
Lone, A.G., Deslandes, V., Nash, J.H., Jacques, M., Macinnes, J.I., 2009. Modulation of gene expression in Actinobacillus pleuropneumoniae exposed to bronchoalveolar fluid. PloS One 4, e6139.
Ludwig, A., Garcia, F., Bauer, S., Jarchau, T., Benz, R., Hoppe, J., Goebel, W., 1996. Analysis of the in vivo activation of hemolysin (HlyA) from Escherichia coli. J. Bacteriol. 178, 5422–5430.
Maier, E., Reinhard, N., Benz, R., Frey, J., 1996. Channel-forming activity and channel size of the RTX toxins ApxI, ApxII, and ApxIII of Actinobacillus pleuropneumoniae. Infect. Immun. 64, 4415–4423.
Malcova, I., Bumba, L., Uljanic, F., Kuzmenko, D., Nedomova, J., Kamanova, J., 2021. Lipid binding by the N-terminal motif mediates plasma membrane localization of Bordetella effector protein BteA. J. Biol. Chem. 296, 100607.
Malherbe, G., Humphreys, D.P., Davé, E., 2019. A robust fractionation method for protein subcellular localization studies in Escherichia coli. BioTechniques 66, 171–178.
Masin, J., Fiser, R., Linhartova, I., Osicka, R., Bumba, L., Hewlett, E.L., Benz, R., Sebo, P., 2013. Differences in purinergic amplification of osmotic cell lysis by the pore-forming RTX toxins Bordetella pertussis CyaA and Actinobacillus pleuropneumoniae ApxIA: the role of pore size. Infect. Immun. 81, 4571–4582.
Matyska Liskova, P., Fiser, R., Macek, P., Chmelik, J., Sykora, J., Bednarova, L., Konopasek, I., Bumba, L., 2016. Probing the Ca(2+)-assisted pi-pi interaction during Ca(2+)-dependent protein folding. Soft Matter 12, 531–541.
McGuffin, L.J., Edmunds, N.S., Genc, A.G., Alharbi, S.M.A., Salehe, Bajuna R., Adiyaman, R., 2023. Prediction of protein structures, functions and interactions using the IntFOLD7, MultiFOLD and ModFOLDdock servers. Nucleic Acids Res. 51, W274–W280.
Meier, R., Drepper, T., Svensson, V., Jaeger, K.E., Baumann, U., 2007. A calcium-gated lid and a large beta-roll sandwich are revealed by the crystal structure of extracellular lipase from Serratia marcescens. J. Biol. Chem. 282, 31477–31483.
Motlova, L., Klimova, N., Fiser, R., Sebo, P., Bumba, L., 2020. Continuous Assembly of beta-Roll Structures Is Implicated in the Type I-Dependent Secretion of Large Repeat-in-Toxins (RTX) Proteins. J. Mol. Biol. 432, 5696–5710.
Nahar, N., Turni, C., Tram, G., Blackall, P.J., Atack, J.M., 2021. Actinobacillus pleuropneumoniae: The molecular determinants of virulence and pathogenesis. Adv. Microb. Physiol. 78, 179–216.
Osicka, R., Prochazkova, K., Sulc, M., Linhartova, I., Havlicek, V., Sebo, P., 2004. A novel "clip-and-link" activity of repeat in toxin (RTX) proteins from gram-negative pathogens. Covalent Protein Cross-Link. Asp. -Lys isopeptide Bond. Calcium-Depend. Process. Asp. -Pro Bond. J. Biol. Chem. 279, 24944–24956.
Osickova, A., Khaliq, H., Masin, J., Jurnecka, D., Sukova, A., Fiser, R., Holubova, J., Stanek, O., Sebo, P., Osicka, R., 2020. Acyltransferase-mediated selection of the length of the fatty acyl chain and of the acylation site governs activation of bacterial RTX toxins. J. Biol. Chem. 295, 9268–9280.
Papadakos, G., Wojdyla, J.A., Kleanthous, C., 2012. Nuclease colicins and their immunity proteins. Q. Rev. Biophys. 45, 57–103.
Persson, C., 2019. Airways exudation of plasma macromolecules: Innate defense, epithelial regeneration, and asthma. J. Allergy Clin. Immunol. 143, 1271–1286.
Ravaud, S., Gouet, P., Haser, R., Aghajari, N., 2003. Probing the Role of Divalent Metal Ions in a Bacterial Psychrophilic Metalloprotease: Binding Studies of an Enzyme in the Crystalline State by X-Ray Crystallography. J. Bacteriol. 185, 4195–4203.
Ristow, L.C., Welch, R.A., 2019. RTX Toxins Ambush Immunity's First Cellular Responders. Toxins (Basel) 11.
Sassu, E.L., Bossé, J.T., Tobias, T.J., Gottschalk, M., Langford, P.R., Hennig-Pauka, I., 2018. Update on Actinobacillus pleuropneumoniae-knowledge, gaps and challenges. Transbound. Emerg. Dis. 65 (1), 72–90.
Schaller, A., Kuhn, R., Kuhnert, P., Nicolet, J., Anderson, T.J., Maclnnes, J.I., Segers, R., Frey, J., 1999. Characterization of apxIVA, a new RTX determinant of Actinobacillus pleuropneumoniae. Microbiology 145 (Pt 8), 2105–2116.
Sheehan, B.J., Bossé, J.T., Beddek, A.J., Rycroft, A.N., Kroll, J.S., Langford, P.R., 2003. Identification of Actinobacillus pleuropneumoniae genes important for survival during infection in its natural host. Infect. Immun. 71, 3960–3970.
Sleytr, U.B., Schuster, B., Egelseer, E.-M., Pum, D., 2014. S-layers: principles and applications. FEMS Microbiol. Rev. 38, 823–864.
Smith, T.J., Sondermann, H., O'Toole, G.A., 2018. Type 1 Does the Two-Step: Type 1 Secretion Substrates with a Functional Periplasmic Intermediate. J. Bacteriol. 200.
Soto Perezchica, M.M., Guerrero Barrera, A.L., Avelar Gonzalez, F.J., Quezada Tristan, T., Macias Marin, O., 2023. Actinobacillus pleuropneumoniae, surface proteins and virulence: a review. Front Vet. Sci. 10, 1276712.
Stancheva, S.G., Frombling, J., Sassu, E.L., Hennig-Pauka, I., Ladinig, A., Gerner, W., Grunert, T., Ehling-Schulz, M., 2022. Proteomic and immunoproteomic insights into the exoproteome of Actinobacillus pleuropneumoniae, the causative agent of porcine pleuropneumonia. Micro Pathog. 172, 105759.
Stanley, P., Packman, L.C., Koronakis, V., Hughes, C., 1994. Fatty acylation of two internal lysine residues required for the toxic activity of Escherichia coli hemolysin. Science 266, 1992–1996.
Stanley, P., Koronakis, V., Hughes, C., 1998. Acylation of Escherichia coli hemolysin: a unique protein lipidation mechanism underlying toxin function. Microbiol Mol. Biol. Rev. 62, 309–333.
Stringer, O.W., Li, Y., Bosse, J.T., Forrest, M.S., Hernandez-Garcia, J., Tucker, A.W., Nunes, T., Costa, F., Mortensen, P., Velazquez, E., et al., 2022. Rapid Detection of Actinobacillus pleuropneumoniae From Clinical Samples Using Recombinase Polymerase Amplification. Front Vet. Sci. 9, 805382.
Venter, A.P., Twelker, S., Oresnik, I.J., Hynes, M.F., 2001. Analysis of the genetic region encoding a novel rhizobiocin from Rhizobium leguminosarum bv. viciae strain 306. Can. J. Microbiol 47, 495–502.
Woida, P.J., Satchell, K.J.F., 2018. Coordinated delivery and function of bacterial MARTX toxin effectors, 107, 133–141.
Yasuta, T., Okazaki, S., Mitsui, H., Yuhashi, K., Ezura, H., Minamisawa, K., 2001. DNA sequence and mutational analysis of rhizobitoxine biosynthesis genes in Bradyrhizobium elkanii. Appl. Environ. Microbiol 67, 4999–5009.
Yuan, F., Liu, J., Guo, Y., Tan, C., Fu, S., Zhao, J., Chen, H., Bei, W., 2011. Influences of ORF1 on the virulence and immunogenicity of Actinobacillus pleuropneumoniae. Curr. Microbiol 63, 574–580.
Zeth, K., Römer, C., Patzer, S.I., Braun, V., 2008. Crystal structure of colicin M, a novel phosphatase specifically imported by Escherichia coli. J. Biol. Chem. 283, 25324–25331.